J Mater Sci (2011) 46:2764–2770
DOI 10.1007/s10853-010-5150-8

Design and characterization of a lamellar nanostructure in a low C steel

S. Allain · M. Gouné · O. Bouaziz · E. Kassir · P. Barges · L. Jantzen

Received: 28 September 2010 / Accepted: 30 November 2010 / Published online: 16 December 2010

Abstract A fully lamellar ferrite/cementite nanostructure was designed in a low C steel by using a specific thermal treatment. The strengthening of such microstructure has been investigated as a function of prestrain by rolling up to a deformation of 300%. As in usual pearlitic structure, its work-hardening shows no saturation and its elongation to fracture remains rather constant instead of decreasing drastically as conventional steels. The hardening by a similitude effect is thus not the privilege of pearlitic steels. Nevertheless, its lower initial work-hardening rate at low strain compared to an equivalent pearlitic steel and a lower hardening potential at high strain let us suspect major differences in the nature and the behaviour of ferrite channels in relation to the morphogenesis of the microstructure. This study opens a new way to obtain low carbon ultra-high strength steel by a nanostructuration process using severe plastic deformations.

Introduction

The refinement of microstructures in steels is a great topic of interest since it is an effective way to develop new generation of steels possessing excellent combination of mechanical properties [1–3]. Fully lamellar pearlite structure, which can be considered as a very fine microstructure, which consists of alternating plates of ferrite and cementite deformed by wire drawing or cold-rolling present an unusual simultaneous increase in strength and an increase in reduction of area explained by the reduction of the scale of the structure, known as the similitude principle, i.e. that the strengthening is mainly controlled by the refinement of the interlamellar spacing geometrically induced by the macroscopic plastic strain [4, 5]. These microstructures lead to impressive mechanical properties. Classically, it is possible to reach strength levels as high as 5.3 GPa [6]. However, in the automotive sector, the wide industrial applications are very limited. Indeed, in order to obtain such microstructures it is a prime of necessity to have high carbon content (around 0.75 wt%) which is detrimental to classical large-scale welding processes as spot welding or as laser welding.

In this article we show that it is possible to design a lamellar nanostructure, which consists of alternating ferrite/carbide lamellae, by using a nominal carbon content lower that the eutectoid composition (i.e. 0.77 wt%C in binary Fe–C) and compatible with the automotive applications. Furthermore, we propose to assess the hardening potential of a such microstructure. A comparison with the mechanical behaviour of pearlitic or ferrite-pearlite steels is proposed.

Experimental procedure

Design of the lamellar nanostructures

For a given composition and cooling rate, it is possible to form a lamellar structure below the eutectoid temperature (around 723 °C in the Fe–C binary) composed by ferrite and aligned cementite precipitation. Indeed, even at low temperature, high driving force for cementite precipitation is available if the carbon composition in austenite exceeds a certain value known as the Hultgren criteria [7]. That carbon composition can be lower than those defined the eutectoid point (around 0.77 wt% in the binary Fe–C) since the transformation occurs out of the thermodynamic equilibrium

S. Allain · M. Gouné (✉) · O. Bouaziz · E. Kassir · P. Barges · L. Jantzen
ArcelorMittal Research, Voie Romaine, BP 30320, 57283 Maizières-lès-Metz Cedex, France
e-mail: Mohamed.Goune@arcelormittal.com

state. To reach that goal it is a prime of necessity to slow down the ferrite kinetics during cooling in order to decrease the temperature of pearlite transformation. Therefore, it is theoretically possible to form a fully "lamellar" microstructure with carbon content and a temperature lower than those defined by the eutectoid point. There is a long standing controversy on the nature of the lamellar structure formation. Ohmori and Honeycombe previously called such microstructure "degenerated pearlite" [8]. Some authors argue this transformation consists of interphase precipitation of cementite and concludes naturally it can be a new variant of bainite especially because its formation temperature is consistent with bainitic transformation [9]. Furthermore, the analysis performed by Lee et al. [10] shows clearly that bainite can adopt different morphologies. They point out that the two major factors which influence the bainite morphology are the ratio of the growth rate of eutectoid ferrite α to that of eutectoid cementite θ and the steady state of the re-nucleation of θ at the α–γ boundary (the austenite matrix phase is designated as γ and the two product phases are θ and α). The product of eutectoid decomposition becomes bainite if the growth rate of eutectoid ferrite is larger than those of eutectoid cementite. When the ratio is not very large, θ should be able to grow alongside of α for some distance. Hence phase θ appears as plates of rods of restricted length. If the re-nucleation of θ at the α–γ boundary increases the degree of alignment between successively formed plates or rods of θ is increased. Higher values of the growth rate of eutectoid ferrite α to that of eutectoid cementite θ and higher value of the steady state of the re-nucleation of θ at the α–γ boundary lead progressively to a finer dispersion of θ in eutectoid α. Then bainite can develop in a wide variety of morphologies. That is why it is sometimes very difficult to make difference between pearlite and bainite. Lastly, others envisage a continuum between lamellar pearlite with plates perpendicular to the growth direction of ledges and upper bainite [11].

But, whatever the considered mechanism, it is clearly possible to promote a lamellar morphology with low nominal carbon content. The selected steel is an alloy containing 0.3 wt%C–3 wt%Mn–1.5 wt%Si. The 2 kg as-cast ingot (20 mm thick) of the given composition has been reheated at 1200 °C during 30 min and hot-rolled down to 3.5 mm with a finish rolling temperature higher than 900 °C to guarantee a fully recrystallized austenitic state prior to the phase transformations. The hot-strip has been then cooled down to 570 °C at a cooling rate of about 50 °C s^{-1} to prevent ferrite formation and put into a furnace at 550 °C to reproduce a coiling stage. The cooling rate down to room temperature is about 20 °C h^{-1}. This thermomechanical treatment leads to the microstructure reported in Fig. 1a. Picral etching was used (4 g acid picric + 100 mL ethanol) to reveal both cementite and ferrite. The microstructure is mainly composed by lamellar ferrite-cementite colonies with a mean interlamellar spacing of 220 nm and very little polygonal ferrite (less than 2%). Even at the Scanning Electron Microscopy (SEM) scale, as the microstructure is fine and etched, it is difficult to estimate directly the volume fraction of carbides. However, from the mass balance equation and by considering the nominal carbon composition in the studied steel, the maximum volume fraction of cementite can be estimated to be 5.6%. Then, it is possible to estimate the cementite plate thickness from the mean interlamellar spacing. Indeed, the cementite plate thickness l_θ can be obtained from the following relation:

$$l_\theta = 2 \times l_s \times f_\theta = 2 \times 220 \times 0.056 = 24.6\,\text{nm}$$

where l_s is the interlamellar spacing, f_θ is the volume fraction of cementite.

As shown in Fig. 1a, the cementite lamellae are mainly discontinuous. One of the possible explanations of that microstructure feature may be explained by considering the results of Lemaire et al. [11]. Indeed, the growth rate of eutectoid ferrite α to that of eutectoid cementite θ and the

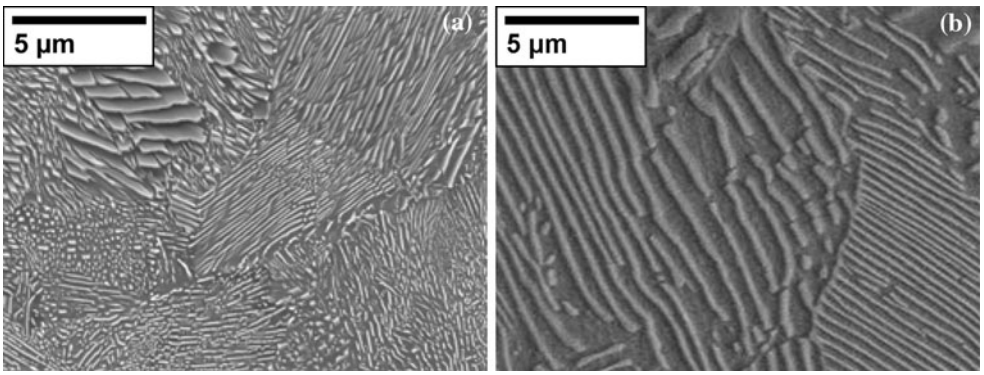

Fig. 1 SEM micrographs after Picral etching of **a** the studied alloy in the as-rolled state and **b** a reference fully pearlitic steel containing 0.7 wt%C. Cementite appears in *bright*

steady state of the re-nucleation of θ at the α–γ boundary influence strongly the resulting morphology and especially, when the ratio is not very large the θ phase appears as plates of rods of restricted length and then the cementite lamellae appear discontinuous. That arrangement of cementite is clearly different of that observed in classical pearlite microstructure represented in Fig. 1b for the sake of comparison.

Assessment of the mechanical performances

Only a severe plastic deformation process with highly compressive components (rolling or extrusion) permits to put into light a similitude effect. In a second processing step, the as-hot rolled strips have thus been cold-rolled up to a total reduction of 93% after numerous passes (from 3 mm gage thickness down to 0.21 mm) on a laboratory mill. Samples have been taken for subsequent tensile tests with different cold-rolling states and thus at different true equivalent prestrain. These true equivalent prestrain levels obtained by rolling can be calculated thank the cold-rolling ratio as follows:

$$\varepsilon = \frac{2}{\sqrt{3}} \ln\left(\frac{1}{1-R}\right) \quad (1)$$

where R is the rolling reduction. A cold-rolling reduction of 93% thus corresponds to a total true equivalent strain of 307%.

Tensile tests have been performed at room temperature with a low strain rate of 10^{-3} s^{-1}. The reductions in area at fracture are measured post-mortem thanks to an optical microscope and an image analysis device.

Results

Evolution of the deformation microstructure

The evolution of the morphology after 86% is reported in Fig. 2. The alignment and the buckling of the lamellae are the main effect of the deformation, as reported classically in usual fully pearlitic steel [12–14]. Traces of a damaging process (microvoids) are visible close to coarse carbides.

Mechanical properties

The stress–strain tensile curves of the studied alloy for the investigated cold reductions are reported in Fig. 3. Without any prestrain by rolling, the tensile curves exhibit a similar behaviour compared to a pearlitic steel with a uniform elongation close to 10% and a rather low work-hardening rate [15, 16] with reference to the other kinds of very high strength steels, as dual-phase steels. After cold-rolling, the tensile curves reach far higher strength but the uniform elongations are reduced drastically as expected (less than 2%).

As shown in Fig. 4, the Ultimate Tensile Strength (UTS) and the Reduction in Area (RA) at fracture increase monotonically as a function of the true equivalent prestrain performed by rolling and no saturation is observed concerning the strengthening even for deformations between 200 and 300%. The RA increases more rapidly from 60 to 80% during the very first levels of prestrains but seems to reach saturation at 80%.

Discussion

Comparison with the behaviour of a pearlitic steel at low strain

The behaviour of the studied alloy without subsequent cold-rolling has been first compared with the the prediction of a model available in the literature for describing the behaviour of a fully pearlitic steel at low plastic strain [16].

The empirical law used to describe the uniaxial behaviour of polycrystalline pearlite has been adjusted on numerous experimental data [12]. The assumption is made that only the ferrite between the cementite lamellae deforms plastically. The initial flow stress is controlled

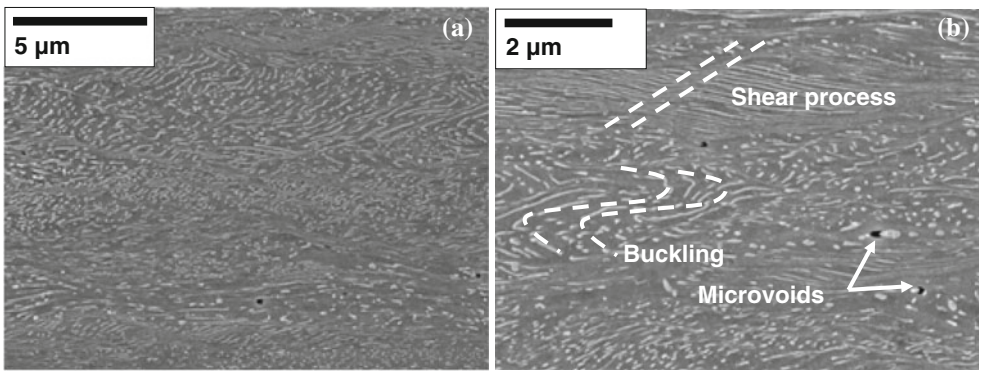

Fig. 2 SEM micrographs after Picral etching of the studied alloy in the cold-rolled state (90% of reduction). Cementite appears in *bright*. Some traces of a damaging process are visible close to coarse carbides

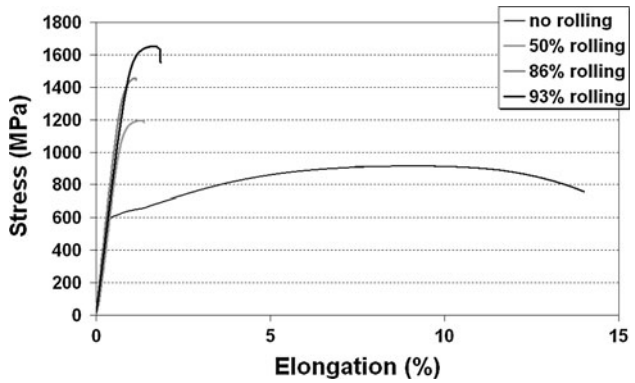

Fig. 3 Engineering tensile curves of the studied alloy after different levels of cold-rolling reduction

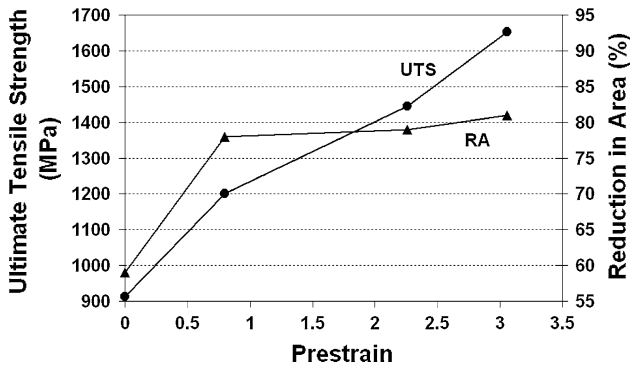

Fig. 4 Evolution of the ultimate tensile strength (*UTS*) and reduction in area (*RA*) at fracture of the studied steel as a function of the true equivalent prestrain by rolling

classically by the interlamellar spacing [4, 15, 16] and plastic work-hardening, considered here as isotropic, and follows a Voce type law without any dependence to the microstructure.

$$\sigma_{\text{pearlite}}\left(\varepsilon_{\text{plastic}}\right) = \sigma_0 + \frac{M\mu b}{S_0} + \frac{K}{g}\left(1 - \exp\left(-g\varepsilon_{\text{plastic}}\right)\right) \tag{2}$$

σ_0 is the critical stress due to the lattice friction in the ferrite lamellae, S_0 is the initial interlamellar spacing, M is the average Taylor factor ($M = 2.77$), μ is the shear modulus (78 GPa) and b is the Burgers vector (2.5×10^{-10} m). K and g are two empirical constants, equal to 38,000 MPa and 70, respectively.

The tensile curves of the studied alloy and of a model pearlite have been represented in Fig. 5 as a function of the true plastic strain. The friction stress for the pearlite has been set to 350 MPa, explained by the high amount of Mn and Si, and the interlamellar spacing to 220 nm as measured experimentally in the studied alloy. The modelled curve will thus represent the behaviour of an equivalent pearlite (same interlamellar spacing but higher fraction of

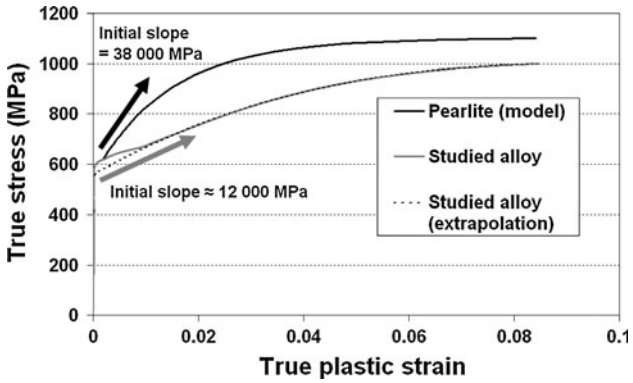

Fig. 5 Comparison between the experimental tensile curve of the studied alloy and the modelled curve of an equivalent pearlitic steel (same interlamellar spacing)

cementite compared to the studied alloy without its degenerated morphology).

Even if both curves show more or less the same behaviour (same UTS, equivalent uniform elongation and yield strengths), they present two distinctive features at low plastic strain. The studied alloy present an obvious Lüders' plateau seldom observed in pearlitic steels and also a far lower initial work-hardening.

For pearlitic steels, the model predicts an initial slope of 38,000 Mpa (Eq. 2). As it is difficult to estimate the initial work-hardening rate of the studied steel due to the presence of the plateau, an extrapolation of the uniform behaviour has been represented in Fig. 5, which gives a far lower value of 12,000 MPa.

The decrease of the initial slope cannot solely be attributed to the decrease of the composite effect due to the lower fraction of elastic component in the microstructure, as:

$$\frac{d\sigma_{\text{studied alloy}}}{d\varepsilon_{\text{plastic}}} \ll \frac{d\sigma_{\text{pearlite}}}{d\varepsilon_{\text{plastic}}} + \left(F^{\text{cementite}}_{\text{studied alloy}} - F^{\text{cementite}}_{\text{pearlite}}\right) \times E = 22,000 \text{ MPa} \tag{3}$$

With E the Young modulus (taken equal to 200 GPa) and considering the following volumes fraction of cementite $F_{\text{pearlite}} = 12\%$ and $F_{\text{studied alloy}} = 4\%$ in the equivalent pearlitic steel and the studied steel, respectively.

It highlights that the behaviour of the channel of ferrite is probably altered in the studied steel compared to pearlite. The channel interface is probably not as perfect as obtained in a perfectly diffusive transformation; it also probably contains higher density of dislocations and different levels of internal stresses due to phase transformation. That explanation is consistent with the fact that transformation occurred at lower temperature than the classical pearlite transformation (around 200 °C of difference). These supposed alterations plead in favour of the bainitic nature of the studied alloy.

Similitude effect at high strain

Highlighting the similitude effect

The similitude effect in pearlitic steels is the strengthening induced by the refinement of the microstructures due to severe plastic deformation under compressive state (rolling or drawing for instance). Considering the pioneer studies of Fischer and Embury [4, 17, 18], the hardness should evolve linearly to the inverse of interlamellar spacing S. During a rolling process, this spacing decreases from S_0 proportionally to a factor $\exp(-\varepsilon/2)$ (ε the equivalent true prestrain). A material showing a similitude effect should thus show a linear dependence of its hardness as function of $\exp(\varepsilon/2)$.

$$\mathrm{H}v\,(\varepsilon) - Hv_0 \propto \frac{1}{S(\varepsilon)} \propto \left(S_0 \exp\left(-\frac{\varepsilon}{2}\right)\right)^{-1} \propto \exp\left(\frac{\varepsilon}{2}\right) \qquad (4)$$

The evolution of UTS measured on the studied alloy after different rolling reduction has been plotted as a function of $\exp(\varepsilon/2)$ (ε the equivalent true prestrain) in Fig. 6. In that particular case, the UTS could be considered as a relevant equivalent to hardness measurements in that case (low uniform elongation but hard strain path change). The UTS determined on as-rolled material—prior to any rolling, i.e. without strain path change—has not been considered in the analysis as the tensile deformation does not induce a similitude effect (contrary to rolling).

An obvious linear trend is observed in Fig. 6 proving that the strengthening by the similitude principle operates in the investigated low carbon lamellar structure. The linear relationship can be expressed as follows:

$$\mathrm{UTS(MPa)} = A + B\exp\left(\frac{\varepsilon}{2}\right) \qquad (5)$$

where A and B have been, respectively, identified to 988 and 145 MPa for the studied alloy.

Equation 2 suggests that in a conventional pearlitic structure, the value of B in Eq. 5 should be approximately given by

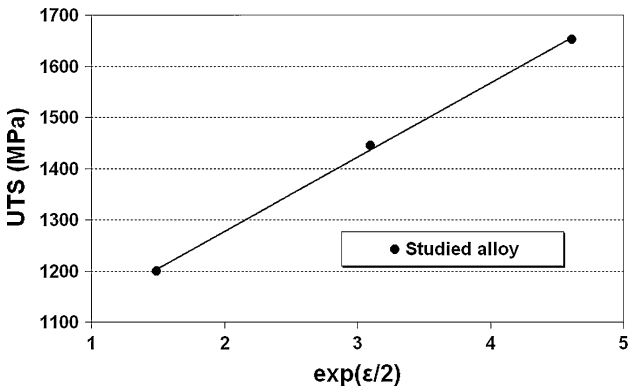

Fig. 6 Illustration of the operating similitude effect on the strengthening by scale refinement for the low carbon lamellar structure

$$B = \frac{M\mu b}{S_0} \qquad (6)$$

A conventional pearlitic structure with the interlamellar spacing S_0 of the studied alloy (220 nm) should have shown a far higher B value (about 245 MPa).

On the contrary, the studied alloy is equivalent to a usual pearlitic with an initial interlamellar spacing of 370 nm concerning the intensity of the strengthening at large plastic strains. The lamellar structure of the studied alloy presents a lower hardening potential than a fully pearlitic structure. This loss of strain-hardening potential is probably due to the discontinuous morphology of the cementite lamellae in the microstructure, which enables relaxation process to occur (due to shear bands as described by Zelin [12] for instance or cementite lath dissolution [19, 20] in fully pearlitic steels).

The another proof of an efficient similitude effect operating during the cold-rolling of the studied alloy is the increase of the reduction in area at fracture (RA%) with strain. The balance between RA% and UTS of the studied alloy at different prestrain levels has been represented in Fig. 7 and compared to the performances of hypereutectoid lamellar pearlitic steel at different drawing levels [21] and of very high strength steels with varying microstructures obtained with similar composition as the studied alloy. The data extracted from Sugimoto et al. [22] are relative to conventional TRIP steel with ferritic matrix, with bainitic matrix and with fibrous annealed martensite matrix, respectively, obtained with a 0.3 wt%C–1.5 wt%Mn–1.5 wt%Si composition. The data extracted from Krauss [23] are relative to a tempered martensitic microstructure with a 4,130 composition.

The Fig. 7 proves not only that the nanostructuration obtained by severe plastic cold-rolling of the studied alloy permits to improve simultaneously its strength and its deformation to fracture but also that the obtained performances of the studied steel prevail over the properties of all the known Very High Strength (VHS) microstructures.

Comparison with an equivalent F + P structure

The strain-hardening after severe plastic deformation obtained by cold-rolling of the studied alloy has been compared to experimental data for pearlitic steel (with a initially small interlamellar spacing 0.1 μm), a fully ferritic steel (low carbon) and a ferrite/pearlite steel with a TRIP composition (about 0.23 wt%C–1.7 wt%Mn–1.6 wt%Si) after [17]. The microstructure of this last steel contains 25% of pearlite (with a large initial interlamellar spacing 0.3 μm).

Also, it is interesting to compare our results (fully pearlitic steels with 0.3 wt%C) with a ferrite/pearlite

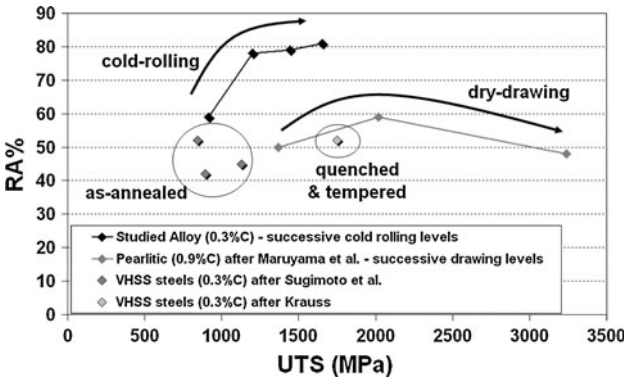

Fig. 7 Evolution of the RA% of the studied alloy as a function of the UTS at the different successive cold-rolling levels. The values are compared to those of a 0.8 wt%C pearlitic steel after [21], conventional 0.3 wt%C TRIP microstructures after [22] and a quenched and tempered 0.3 wt%C martensitic steel after [23]

microstructure having the same level of carbon. However, to our knowledge, no data are available in the literature; that is why a model developed and successfully used by [17] has been applied to estimate the mechanical properties at high strain of an equivalent ferrite/pearlitic with the composition of the studied alloy.

During the ferrite formation during cooling, when the carbon composition exceeds a certain value (known as the Hutgren criteria), high driving force is available for cementite precipitation. It corresponds to the extrapolation of the $\gamma + \theta$ at low temperature (usually named Aecm). This criterion is usually used to determine the carbon composition in austenite and temperature for pearlite formation. By using thermocalc under paraequilibrium it is possible to calculate the Aecm curve. Indeed, Hillert [24] discussed the growth conditions for pearlite under quasi-paraconditions and concludes that the necessary diffusion of Mn is so slow that the carbon activity has an almost constant value along the pearlite/austenite interface. As a consequence, the growth of pearlite under paraequilibrium condition can be considered and it seems reasonable to conclude that the growth rate may still be limited mainly by the rate of carbon diffusion. The corresponding volume fraction of pearlite can be obtained by a mass balance. Then it is possible to design a temperature for a given volume fraction of pearlite. In our case, the calculations show at 650 °C, the carbon composition in austenite for pearlite formation is 1.3 wt%C and the corresponding volume fraction of pearlite is 23%.

In order to determine the interlamellar distance S_0, we use the equation proposed by Marder and Bramfitt [25]:

$$S_0(\text{nm}) = \frac{8020}{\Delta T} \tag{7}$$

At the given temperature of 650 °C, the undercooling ΔT is 73 K which leads to an interlamellar distance of 115 nm.

The evolutions of the UTS of the studied alloys and selected comparison steels as a function of the equivalent prestrain obtained by rolling and the deduced mean strain-hardening evolutions are represented in Fig. 8a and b, respectively.

As discussed in the previous section, the strain-hardening shown by the studied alloy at high strain is far lower than optimal fully pearlitic steel, but is twice higher than the equivalent ferrite/pearlite microstructure with 0.3 wt%C. The pearlite fraction in this model steel is insufficient to sustain the strain-hardening at high strain, which will saturate (about to 100 MPa). On the contrary, the fully lamellar structure in the studied steel permits to expect a continuous increase in the strain-hardening (macroscopic similitude effect).

Conclusion

A fully lamellar ferrite/cementite nanostructure was designed in a low C steel. The carbon content and the

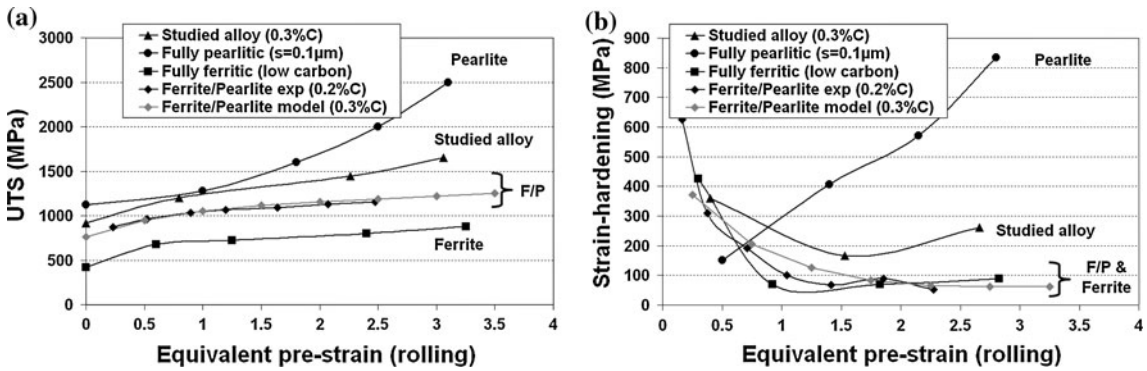

Fig. 8 **a** Evolutions of the UTS and **b** of deduced strain-hardening of the studied alloy and selected comparison steels (experimental and modelling results) as a function of the equivalent prestrain obtained by rolling

temperature of formation of such nanostructure are below those defined by the eutectoid point.

The strengthening has been investigated as a function of prestrain by rolling up to a deformation of 300%. Prior to rolling, the tensile behaviour of the studied alloy looks like the one of a usual pearlitic steel. Nevertheless, its low initial work-hardening let us suspect that the nature of the ferrite lamellae is probably bainitic or altered.

The studied alloy presents a strengthening behaviour at high strain consistent with a similitude effect usually operating in eutectoid pearlitic structures but less efficient due probably to the discontinuous morphology of its cementite lamellae. Its strain-hardening values are estimated to be twice higher than an equivalent ferrite/pearlite microstructures obtained with a similar composition. Its increase in strength by successive cold-rolling operations goes together with an increase in the deformation to fracture as in usual pearlitic steels. Its performance ductility/strength overcomes the properties of all the known VHS microstructures that could be obtained with the same compositions.

From a more practical point of view, a new way has thus been identified to produce low carbon nanostructured ultra-high strength steel by the mean of a severe plastic deformation process compatible with a more massive production.

References

1. Rodriguez-Baracaldor R, Benito JA, Cabrera JM (2010) J Mater Sci 45:4796. doi:10.1007/s10853-010-4600-7
2. Calliari I, Brunelli K, Zanellato M (2009) J Mater Sci 44:3764. doi:10.1007/s10853-009-3505-9
3. Okitsu Y, Takata N, Tsuji N (2008) J Mater Sci 43:7391. doi:10.1007/s10853-008-2971-9
4. Embury JD, Fisher RM (1966) Acta Metall 14:147
5. Goto S, Kirchheim R, Al-Kassab T, Borchers C (2007) Trans Nonferrous Met Soc China 17:1129
6. Lesuer DR, Syn CK, Sherby OD, Kim DK (1997) In: Paris HG, Kim DK (eds) Metallurgy processing and applications of metal wires. TMS, Warrendale, PA
7. Hultgren A (1947) Trans ASM 39:915
8. Ohmori Y, Honeycome RWK (1971) Suppl Trans ISIJ 11:1460
9. Kamat RG, Hawbolt EB (1994) Can Metall Q 33:121
10. Lee HJ, Spanos G, Shiflet GJ, Aaronson HI (1988) Acta Metall 36:1129
11. Lemaire E, Copreaux J, Roch F (1996) Scr Mat 35:83
12. Zelin M (2002) Acta Mater 50:4431
13. Nam WJ, Bae CM (1995) Mater Sci Eng A 203:278
14. Zhang X, Godfrey A, Hansen N, Huang X, Liu W, Liu Q (2010) Mater Char 65
15. Dollar M, Bernstein IM, Thompson AW (1988) Acta Metall 36:311
16. Allain S, Bouaziz O (2008) Mater Sci Eng A 496:329
17. Bouaziz O, Lecorre C (2003) Mater Sci Forum 426–432:1399
18. Gil Sevillano J (1991) J Phys III 1:967
19. Languillaume J, Kapelski G, Baudelet B (1997) Mater Lett 33:241
20. Danoix F, Julien D, Sauvage X, Copreaux J (1998) Mater Sci Eng A 250:8
21. Maruyama N, Tarui T, Tashiro H (2002) Scr Mater 46:599
22. Sugimoto K, Kanda A, Kikuchi R, Hashimoto S, Kashima T, Ikeda S (2002) ISIJ Int 42(8):910
23. Krauss G (1999) Mater Sci Eng 273–275:40
24. Hillert M, Aaronson HI, Laughlin DE, Sekerka RF, Wayman CM (1982) Solid–solid phase transformations. AIME, Warrendale, PA, p 789
25. Marder AR, Bramfitt BL (1975) Metall Trans A 6:2009